Squeeze flow in heterogeneous discontinuous viscous woven prepreg laminates

Experimental measurements and 3D modeling

Grégoire Sorba [1], **Christophe Binetruy** [1], **Adrien Leygue** [1], **Sandeep Gudiwada** [1], **Jean-Michel Lebrun** [1], **François Bertrand** [1], **Sébastien Comas-Cardona** [1], **Thomas Jollivet** [2]

1. *GeM - Research Institute of Civil Engineering and Mechanics, UMR 6183, CNRS, École Centrale de Nantes - Université de Nantes*
   1 rue de la Noë
   F-44321 Nantes CEDEX
   {gregoire.sorba,christophe.binetruy,adrien.leygue,jean-michel.lebrun,francois.bertrand,sebastien.comas}@ec-nantes.fr,sandeep.gudiwada@eleves.ec-nantes.fr
2. *CETIM / Pôle Ingénierie Polymères et Composites*
   Technocampus EMC2, Z. I. du Chaffault
   F-44340 Bouguenais
   thomas.jollivet@cetim.fr

ABSTRACT. *Thermoplastic matrix composites reinforced with glass fiber reinforcements are viewed as an alternative to thermoset matrix composites for structural components in the automotive field, as they allow for lower costs and higher production rates. However, the forming of thermoplastic composites from a preform made of discontinuous plies is more sensitive to some defects, among which disorientation of the reinforcements originating from the bending and / or solid rotation of a discontinuous ply. These defects result from the polymer movements induced by the consolidation of the composite and degrade mechanical properties. For this reason, anticipating the risk of disorientation of the reinforcements during the manufacturing process is necessary to optimize the mechanical efficiency of the manufactured parts. This paper presents experiments conducted to identify the behavior of a stack of woven prepregs under compression and then proposes a model based on laminated isotropic and anisotropic fluid approach to describe and simulate this behavior numerically. Finally, experiments and simulations are compared to verify the validity of the model.*

RÉSUMÉ. *L'industrie automobile s'intéresse aux composites à matrice thermoplastique à renforts en fibres de verre comme alternative aux composites à matrice thermodurcissable pour les*

composants structuraux dans le domaine automobile, car cela permet des coûts réduits et des cadences de production plus élevées. Cependant la mise en forme de composites thermoplastiques à partir d'une préforme consituée de plis discontinus est plus sensible à certains défauts, parmi lesquels la désorientation des renforts provenant de la flexion et/ou de la rotation solide d'un pli discontinu. Ces défauts résultent des mouvements du polymère induits par la consolidation du composite et conduisent à des chutes de propriétés mécaniques. Pour cette raison, anticiper le risque de désorientation des renforts durant le procédé de fabrication est nécessaire pour optimiser le rendement mécanique des pièces fabriquées. Cet article présente des expériences conduites pour identifier le comportement d'un empilement de préimprégnés tissés sous compression, puis propose un modèle basé sur une approche d'empilement de couches de fluide anisotrope et isotrope pour décrire et simuler ce comportement numériquement. Finalement les expériences et les simulations sont comparées pour vérifier la validité du modèle.

KEYWORDS: *anisotropic fluid, thermoplastic woven prepreg, consolidation, squeeze flow.*

MOTS-CLÉS : *fluide anisotrope, préimprégné thermoplastique, tissé, écoulement, compression.*

DOI:10.3166/RCMA.28.35-53 © 2018 Lavoisier

1. Introduction

Fiber reinforced composites present the important advantage of the design flexibility. They can be shaped in very complex forms to meet design requirements starting from a prepreg material that is a flat sheet that combines fibers and thermoplastic or uncured thermoset matrix. To get a 3D part, the initially planar prepreg is formed into a final 3D shape during forming using the thermo-stamping process. In order to keep the design flexibility, the main concern is then to control the fiber orientation and reduce the remaining defects under an acceptable level, while keeping the target cycle time.

Table 1 reports the most frequent defects observed during the thermo-stamping of melt thermoplastic prepregs, including those processed with the Quilted Stratum Process (QSP®) presented by Schell *et al*. (2016). They are listed in the decreasing level of severity. These defects were also presented by Guillon *et al*. (2016).

The interlaminar shear effects play a significant role in the forming of multi-layered composite parts. Due to its important lubrication function, the thermoplastic matrix decreases interply friction and therefore facilitates large rotation of discontinuous plies. Interply-slip helps to alleviate the compressive stresses, and fiber waviness or even fiber buckling can be avoided. A resin rich layer exists in between prepreg plies, where the two resin rich layers on either side can represent about 5% of the total thickness (Cogswell, 2013). It affects the outcome of forming processes (McGuinness, Ó Brádaigh, 1997) (McEntee, Ó Brádaigh, 1998).

The production of quality part without extensive experimental investigations is needed. Then it is important to know in advance where issues during forming may occur and how they can be solved. Designing the process through a trial and error procedure may lead to an acceptable product, but it always brings additional labor costs, machine time, tooling costs and scraps. Due to the complexity of the prob-

Table 1. Most frequent defects observed in the thermo-stamping of thermoplastic viscous prepregs, including those obtained with the Quilted Stratum Process (QSP®)

Defects	Most frequent origin	Mechanical influence on composites
In-plane fiber waviness	– Friction on tooling – Inter-ply friction – In-plane compression of prepregs – Transverse squeeze flow	– Local stiffness weakening – Reduction of tensile and compression strength – Higher risk of local buckling
Off-plane fiber waviness	– Buckling of fibers in part radii – Ply washing due to high injection pressure during overloading	– Local stiffness weakening – Reduction of tensile and compression strength – Higher risk of local buckling
Wrinkles	– High shearing in 3D shape – Lack of room in the mold cavity	– Equivalent to a broken ply
Delamination	– Inappropriate thermal management of the process	– Bending strength weakening
Incomplete impregnation	– Pre-existing defect in prepregs	– Early transverse cracking
Porosities	– Too much moisture in polymer	– Weak effect due to the high toughness of thermoplastics
Residual stresses	– Thermal mismatch between fiber and matrix – High chemical shrinkage of polymer	– Overloading conditions in some areas of the part

lem, the numerical simulation of the forming of complex blanks can be of great help. Numerical tools can simulate the production processes and provide to the subsequent FEA a material-scale description of the "as-manufactured" part. The in-plane loading and slip of a UD prepreg ply has been modeled in (Sorba *et al*., 2016).

In this paper the solid body rotation of a discontinuous woven fiberglass prepreg under compression will be investigated experimentally in Section 3., then a model based on a fluid approach will be presented in Section 4. and finally numerical simulations will be conducted and compared to the experimental results in Section 5..

2. Experimental setup

2.1. Material

The first material used is the Dupont™ Vizilon™ VZLSU75G1 T1.5-1H. It is a 4-1 biased plain weave glass fabric (it has 80% of fibers in the warp direction and 20% of fibers in the weft direction) reinforced polyamide 66-6 prepreg material. Based on the respective fiber content in the warp and the weft directions, this material is intermediate between the woven and the unidirectional prepregs. The laminated preconsolidated prepreg sheet has a fiber volume fraction of 57%, density of 1.98 $\mathrm{g.cm^{-3}}$ and a thickness of 1.60 mm. The melting temperature of the polyamide matrix used is 260 °C.

2.2. Test specimens

The test specimen is made by stacking three plies of preconsolidated prepref of size 150 x 150 $\mathrm{mm^2}$ with two stacking sequences (0 ° ply, angle ply, 0 ° ply) where 20 ° and 80 ° angles were considered. The plies are cut accordingly to their respective angle 0 °, 20 ° or 80 °. Some copper wires of 0.1mm in diameter are placed along the fiber directions to form a 80 x 80 $\mathrm{mm^2}$ grid in two of the plies in each specimen to track the inter-ply flow and investigate the final orientation of the fibers after the compaction (Figure 1a). The final thickness of the specimen is 5mm. The copper wires are not inserted at the same interface as they would significantly increase the interface thickness and also increase the friction between due to the copper-copper friction when subjected to rotation or move, leading to incorrect results. The ply edges are left unconstrained to let the fibers expand and rotate/bend. An example of the final specimen is shown in Figure 1b.

2.3. Test procedure

A compaction force of 100 kN was applied on the specimen where the mold plates are pre-heated for the material to reach 260°C in a monotonous way for preconsolidation to debulk the material and ensure some welding of the plies without inducing squeeze-flow. The square specimen is placed inside the press with spacers of thickness 4.9 mm to control the thickness of the compressed specimen. It is maintained at the melting temperature for 5 min and finally cooled down gradually. The test specimen is then removed out from the hot-press and subjected to optical inspection through X-Ray micro-Computer Tomography (CT) before compaction to map the initial orientation of copper wires inside the specimen. The specimen is then re-heated

(a) Laying of copper wires along the fiber direction. (b) Specimen after compression

Figure 1. Illustration of the test specimen

to 260°C and subjected to compression at 400 kN for 5 minutes, with spacers to control the final thickness, and then cooled down gradually. A final optical inspection is then realized to map the final orientation of copper wires. This is done to investigate the fiber rotation as the pressure due to the normal compressive load makes the molten polymer squeeze and flow, which makes the fiber rotate and/or bend. The angles between the copper wires are measured before and after the compaction to measure the rotation of the fibers. This rotation occurs if the material is completely melted, therefore the behavior is affected by the viscosity at the melted state and not by the subsequent cooling rate.

3. Experimental observations

3.1. $\{0, 20, 0\}$ stack

An assembly of one 20 ° orientation ply in between two zero degree plies was compressed. Measured rotation values are presented in Table 2.

Table 2. Angles for the $\{0, 20, 0\}$ stack

Label	Before	After	Difference	Label	Before	After	Difference
A	19.9	18.1	-1.8	G	22.6	31.3	8.7
B	17.0	34.6	17.6	H	20.4	22.2	1.8
C	18.7	36.4	17.7	I	18.3	24.7	6.4
D	17.0	38.5	21.5	J	20.6	20.29	-0.31
E	25.9	27.4	1.5	K	20.8	24.6	3.8
F	15.4	17.9	2.5				

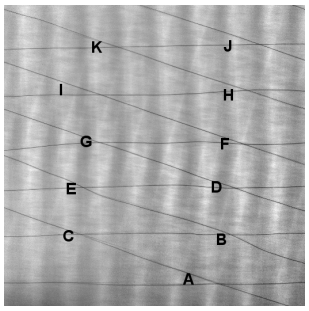

(a) Orientation of wires before compression.

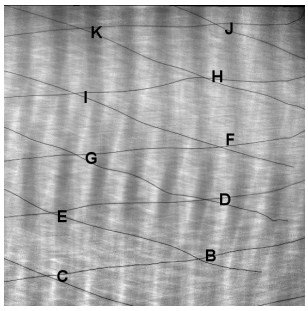

(b) Orientation of wires after compression.

Figure 2. CT-scan of the $\{0, 20, 0\}$ specimen

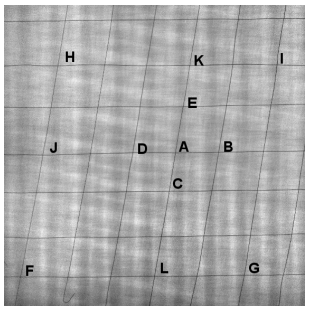

(a) Orientation of wires before compression.

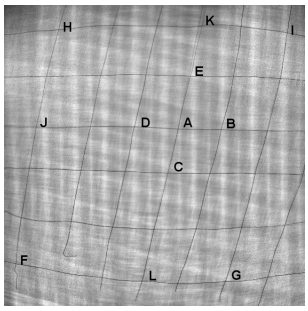

(b) Orientation of wires after compression.

Figure 3. CT-scan of the $\{0, 80, 0\}$ specimen

Measurements give the evidence that the middle layer rotates with respect to the two outer plies. This is a phenomenon that was seen in angle-ply laminated made of unidirectional prepregs. It can be seen that fibers bent at the edges of the composite due to the resin flow towards the edges which modifies the orientation near the edges. The copper wires after compression show a certain degree of waviness, likely due to the crimp in the woven fabric.

3.2. $\{0, 80, 0\}$ stack

An assembly of one 80° orientation ply in between two zero degree plies was compressed. Measured rotation values are presented in Table 3.

The same phenomenon of fibers bending can be seen near the edges. As it can be seen from Table 3, there is closing of the fibers when subjected to compression.

3.3. Conclusion

The above CT-images in Figures 2a to 3b and the measured angles show that the fibers have opened i.e. rotated in the anti-clockwise direction in the $\{0, 20, 0\}$ stack,

Table 3. Angles for the $\{0, 80, 0\}$ stack

Label	Before	After	Difference	Label	Before	After	Difference
A	80.3	77.9	-2.4	G	79.6	67.5	-12.1
B	78.2	76.0	-2.2	H	78.1	67.9	-10.2
C	80.6	76.5	-4.1	I	82.5	91.1	8.6
D	80.3	76.7	-3.6	J	78.6	81.2	2.6
E	79.7	76.3	-3.4	K	80.0	74.7	-5.3
F	79.0	94.4	15.4	L	79.2	79.6	0.4

while in the $\{0, 80, 0\}$ stack most of the fibers have closed. The size effect is seen dominant as the fiber orientation is disturbed by the resin flow towards the edges due to this the fibers are bent around the edges and the orientation is disturbed. The fibers at the center are less impacted since they are less subjected to fiber bending. This shows the size effect of the plies on the fiber orientation in composites processing of discontinuous prepregs. No intra-ply shear was observed, which validates the approach of modeling the woven prepreg as a stack of two cross-ply unidirectional prepregs.

3.4. Influence of the specimen size

In the previous experiments specimens of size 150 x 150 mm^2 are examined for the assessment of fiber rotation under compaction of 100 kN with no edges being constrained. Due to the fiber rotation in the edges as a result of transverse polymer flow, the fiber orientation is disturbed to some extent. Assuming that the size effect has an influence on the rotation of the fibers, further examination was conducted on larger specimens of size 300 x 300 mm^2 with a grid size of 80 x 80 mm^2 at the centre of the specimen. The copper wires are laid in the grid along the fiber direction, and the copper grid in the angle ply is laid along the fibers in the ply as the 300 x 300 mm^2 ply is cut at particular angle [20°\45°] accordingly. Two prepreg materials are used in order to investigate the fiber rotation in both unbalanced and balanced woven fabrics. The same test procedure is followed as explained in the Section 2.3..

The preconsolidated prepreg sheets used for the experiments are described in Table 4.

Table 4. Properties of the Vizilon™ prepreg sheets

Property	Vizilon™ SU75G1	Vizilon™ SB75G1
Fabric	4-1 biased plain weave	2-2 twill weave
Warp / weft ratio (%)	80 / 20	50 / 50
Thickness (mm)	1.6	
Fiber mass fraction (%)	75	
Fiber volumic fraction (%)	57	
Density ($\mathrm{g.cm}^{-3}$)	1.98	
Melting temperature (°C)	260	

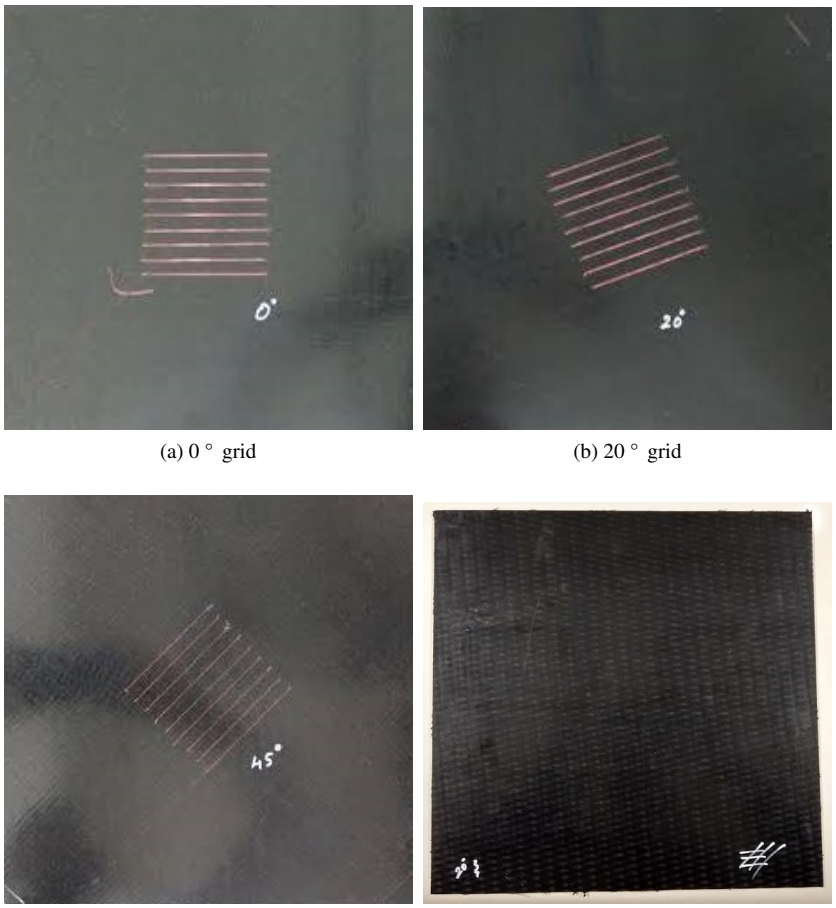

(a) 0 ° grid (b) 20 ° grid

(c) 45 ° grid (d) Final specimen

Figure 4. Illustration of the different grid lay ups

The overall fiber content and resin content is the same for both prepregs, they differ by the way the two constituents are distributed. This experiment with the above two prepeg materials will also helps us to investigate the influence of the polymer/fiber distribution on the fiber rotation.

3.4.1. Vizilon™ SU75G1 prepreg

3.4.1.1. $\{0, 20, 0\}$ stack

An assembly of 20° orientation ply in between two 0° plies of the prepreg Vizilon™ SU75G1 was compressed under a pressure of 0.5 MPa at the melting temperature. Measured rotation values are presented in Table 5. The angles measured here are the obtuse angles at the points labelled in Figure 5.

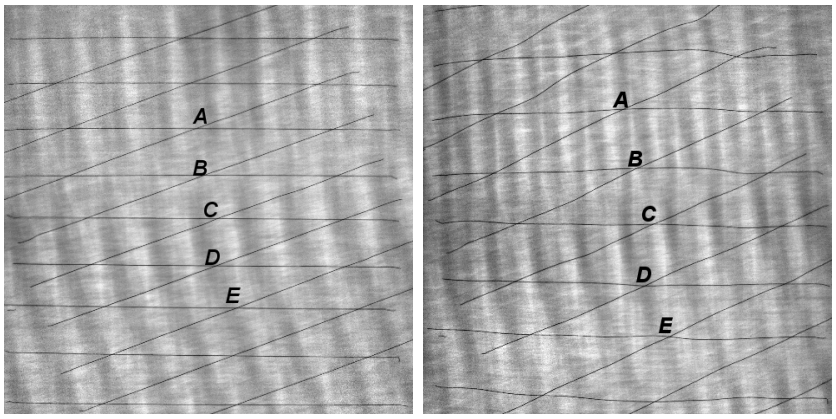

(a) Before compression. (b) After compression.

Figure 5. CT-scan of $\{0°, 20°, 0°\}$ *specimen*

Table 5. Initial and after compression at 0.5 MPa *angles for the* $\{0°, 20°, 0°\}$ *stack*

Label	Initial	Final
A	159	152.3
B	159.6	153.7
C	159.7	156.6
D	159.7	157.5
E	159	154.6

It can be seen in Table 5 that the fibers have rotated and that there is an overall 4.46° rotation of fibers on average. However at point C in the center of the grid and the composite, a minimum rotation of 3.1° is observed. A slight bending at the edges of the grid confirms that the polymer flows towards the sample edges when subjected to compression.

3.4.1.2. $\{0, 45, 0\}$ stack

An assembly of 45° ply in between two 0° plies of the Vizilon™ SU75G1 was compressed at a pressure of 0.5 MPa at the melting temperature. Measured rotation values are presented in Table 6.

It can be seen from Table 6 that the fibers have rotated, and that there is an overall 4.8° rotation of fibers on average. It can be seen that the copper wires remained comparatively straight as of the initial orientation.

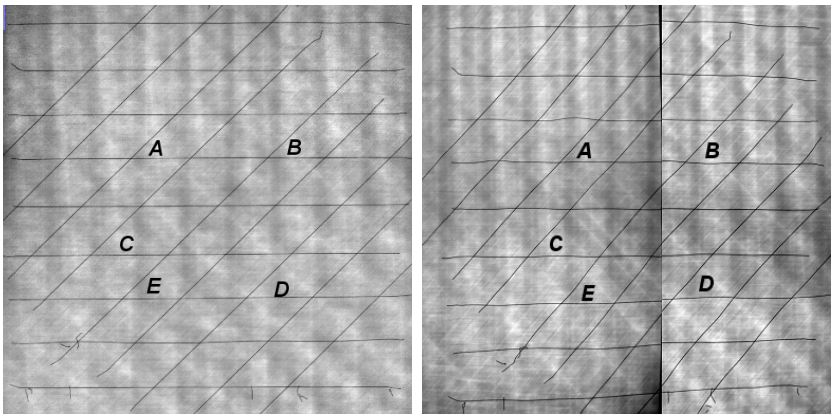

(a) Before compression. (b) After compression.

Figure 6. CT-scans of $\{0°, 45°, 0°\}$ *specimen*

Table 6. Initial and after compression at 0.5 MPa *angles for the* $\{0°, 45°, 0°\}$ *stack*

Label	Initial	Final
A	43.6	48
B	43.4	47.2
C	43.2	47.7
D	43.4	47.5
E	43.5	50.7

3.4.2. Vizilon™ SB75G1 prepreg

3.4.2.1. $\{0, 20, 0\}$ stack

An assembly of 20° oriented ply in between two 0° plies of the Vizilon™ SB75G1 was compressed at a pressure of 0.5 MPa at the melting temperature. Measured rotation values are presented in Table 7. The angles measured here are the obtuse angles at the points labelled in Figure 7.

Table 7. Initial and after compression at 0.5 MPa *angles for the* $\{0°, 20°, 0°\}$ *stack*

Label	Initial	Final
A	160	159.7
B	160.2	159.3
C	160.7	160.4
D	160.5	160
E	160.6	160

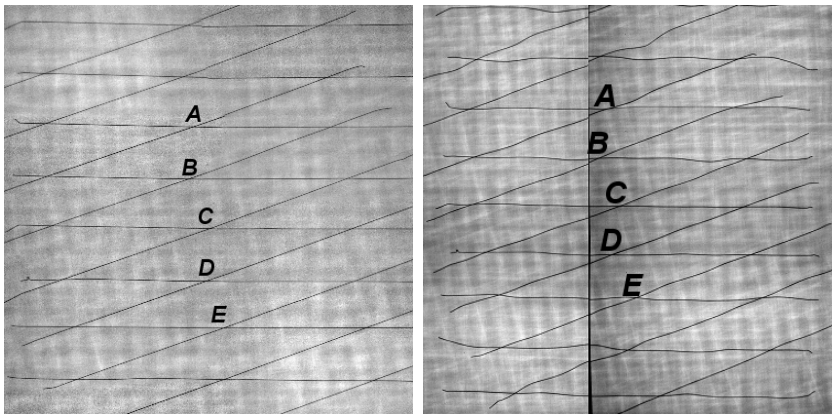

(a) Before compression. (b) After compression.

Figure 7. CT-scan of $\{0°, 20°, 0°\}$ specimen

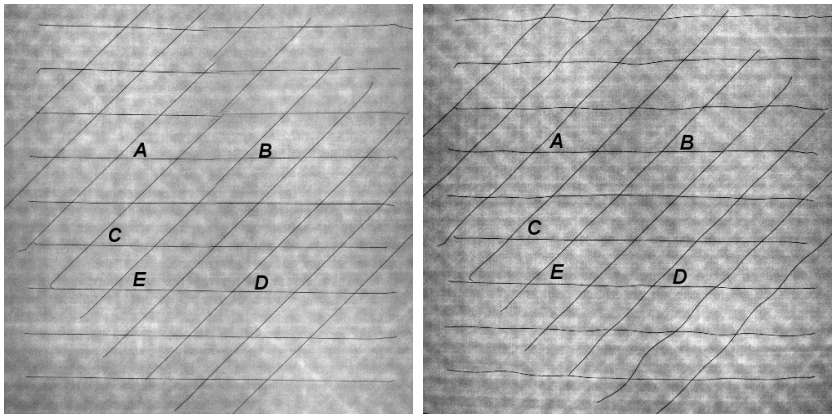

(a) Before compression. (b) After compression.

Figure 8. CT-scan of $\{0°, 45°, 0°\}$ specimen

It can be seen from Table 7 that there is almost no rotation of the fibers, which indicates that the balanced/unbalanced nature of the prepreg has an influence on the solid body rotation.

3.4.2.2. $\{0, 45, 0\}$ stack

An assembly of 45° oriented ply in between two 0° plies of the Vizilon™ SB75G1 was compressed at a pressure of 0.5 MPa at the melting temperature. Measured rotation values are presented in Table 8.

Table 8. Initial and after compression at 0.5 MPa *angles for the* $\{0°, 45°, 0°\}$ *stack*

Label	Initial	Final
A	45	45.3
B	45	45.8
C	45	45.2
D	45.4	46.5
E	45	45.4

It can be seen from Table 8 that there is almost no rotation of fibers.

3.5. Conclusion

The bending of the central fibers is not seen in the larger specimen. It is also noticed that the copper wires are wavy at some points, which is likely due to the crimp in the woven fabric. No intra-ply shear was observed, which validates the approach of modeling the woven prepreg as a stack of two cross-ply unidirectional prepregs.

Figures 5b, 6b, 7b and 8b revealed there is no bending of the copper wires in the grid directed towards the edges, which means that the rotation of the fibers is influenced by the size effect.

Upon detailed observation, it can be seen that the rotation of the fibers in the balanced prepreg is much less than in the unbalanced prepreg. On an average the fibers in the balanced prepreg fabric underwent a rotation of 0.52° in [0°, 20°, 0°] orientation and 0.56° in [0°, 45°, 0°] orientation, while the fibers in the unbalanced prepreg fabric experienced an average rotation of 4.46° in [0°, 20°, 0°] orientation and 4.8° in [0°, 45°, 0°] orientation. It is believed that the asymmetric flow of polymer in the unbalanced prepreg is the origin of this solid body rotation.

4. Model

The Transversally Isotropic Fluid (TIF) model has been developed on the basis of the elastic ideal fiber reinforced model proposed by Pipkin and Rogers (1971) and Spencer (1972). This work was adapted by Rogers (1989) to the case of viscous composites in order to simulate the forming process of a stack of composite plies. The melted resin is considered as a viscous incompressible fluid, and the presence of fibers is taken into account by adding an inextensibility constraint in the fiber direction, leading to an homogenized, transversely isotropic, incompressible and inextensible viscous fluid. It is a fully predictive model based on properties such as fiber volume fraction and resin viscosity. It is attractive because it reduces the need for extensive characterization campaign.

As the rate of deformation during the process is slow enough, the non-linear dynamic effect are not taken into account and the viscosity of the thermoplastics is supposed to be independent of the shear rate. Based on that hypothesis, the homogenized fluid is considered in a succession of quasi-static states. Therefore the simulation con-

sists of computing the instantaneous velocity, then updating the geometry of the stack of plies and the fiber orientation before going on to the next time step.

Previous attempts to model woven fabric using the TIF model by Ghnatios *et al*. (2016) consisted in adding to the viscosity matrix a second fiber direction. In this paper a woven fabric ply will be modeled as a stack of two discontinuous unidirectional plies, with the thickness ratio between the two layers chosen to respect the volumetric ratio between the two fiber directions of the woven fabric. This approach is motivated by the observation that the particular woven used during the experimentations has a structure between the balanced woven prepreg and the unidirectional prepreg.

4.1. Kinematic constraints

The modeled fiber-aligned prepreg material has a viscous behavior coupled with an incompressibility and an inextensibility in the fiber direction, as discussed by Rogers (Rogers, 1989). The incompressibility can be written under the form proposed in (1), and the inextensibility in the fiber direction under the form introduced in (2).

$$\underline{\nabla} \cdot \underline{V} = 0 \tag{1}$$

$$\underline{a}^T \left(\underline{\underline{\nabla}}^S \underline{V} \right) \underline{a} = 0 \tag{2}$$

with $\underline{a}$ the orientation vector of the fibers defined in (3) and $\underline{\underline{\nabla}}^S \underline{V}$ the velocity gradient tensor defined in (4), also referred to as $\underline{\underline{\dot{\varepsilon}}}$.

$$\underline{a} = \begin{bmatrix} \cos(\theta) \\ \sin(\theta) \\ 0 \end{bmatrix} \tag{3}$$

$$\underline{\underline{\nabla}}^S \underline{V} = \frac{1}{2} \left(\frac{\partial \underline{V}}{\partial \underline{x}}^T + \frac{\partial \underline{V}}{\partial \underline{x}^T} \right) \tag{4}$$

4.2. Constitutive model of viscous unidirectional composite

The assumption the fibers are straight and parallel and stay in the plane of the ply is made as discussed by Rogers in (Rogers, 1989). These considerations lead to the behavior law expressed in (5).

$$\underline{\underline{\sigma}} = \underline{\underline{\underline{D}}} \, \underline{\underline{\dot{\varepsilon}}} - P \underline{\underline{1}} + T \underline{a} \otimes \underline{a} \tag{5}$$

with $\underline{\underline{\underline{D}}}$ the transversely isotropic viscosity tensor explicited in (6), $\underline{\underline{\dot{\varepsilon}}}$ the rate of strain tensor, P the pressure and T the tension in the fibers.

$$\underline{\underline{\underline{D}}} = 2\eta_T \underline{\underline{1}} + 2\left(\eta_L - \eta_T\right) \underline{a} \otimes \underline{a} \tag{6}$$

The equation (6) defines an anisotropic fluid of viscosity η_L along the fiber direction and η_T in the other principal directions, corresponding to the desired behavior for the TIF model.

4.3. Update of the geometry

4.3.1. Mesh position

Once the velocity known, the position of the mesh can be updated using an explicit scheme as shown in (7).

$$\underline{x}_{i+1} = \underline{x}_i + \Delta t\, \underline{V}_i \tag{7}$$

The inextensibility constraint being enforced upon the instantaneous velocity, this condition becomes unfulfilled as soon as the mesh is modified. Therefore, a special attention is paid on the quality of the computation due to the use of an explicit scheme instead of an implicit one, and the stability of the method should be verified.

4.3.2. Fiber reorientation

Assuming that the fibers' orientation varies with the resin during the transformation, the fiber rotation equation can be given as (8), as discussed by Rogers (Rogers, 1989).

$$\frac{D\underline{a}}{Dt} = \left(\underline{\underline{\nabla}}\, \underline{V}\right) \underline{a} \tag{8}$$

Injecting (3) into (8) and expressing $\dot{\underline{a}}$ and $\underline{a}$ in terms of $\dot{\theta}$ and θ leads to

$$\begin{aligned}\dot{\theta} = \Bigg(\cos^2(\theta)\left[\left(\frac{\partial V_x}{\partial x}\right)^2 + \left(\frac{\partial V_y}{\partial x}\right)^2\right] + \sin^2(\theta)\left[\left(\frac{\partial V_x}{\partial y}\right)^2 + \left(\frac{\partial V_y}{\partial y}\right)^2\right] \\ +2\cos(\theta)\sin(\theta)\,\frac{\partial V_x}{\partial x}\frac{\partial V_x}{\partial y}\frac{\partial V_y}{\partial x}\frac{\partial V_y}{\partial y}\Bigg)\end{aligned} \tag{9}$$

Equation (9) can be injected into an explicit update scheme in order to obtain the variation of the fiber orientation as in (10).

$$\theta_{n+1} = \theta_n + \Delta t.\dot{\theta} \tag{10}$$

4.3.3. Choice of elements

It is discussed by Hughes (1974) that the shape functions for velocity should be of a higher order than the shape functions for the lagrangian multiplier associated with the incompressibility constraint in order to avoid locking, and this assumption was made for the inextensibility constraint as well. Quadratic shape functions are therefore used

for interpolating the velocity whereas linear shape functions are used for interpolating the pressure and the fiber tension, leading to the choice of the H27-8-8 elements, containing 27 velocity nodes and 8 pressure/tension nodes.

5. Results

In order to compare the model to the experimental observations, simulations were carried out on the two test specimens descibred in Section 2.2.. To model the woven prepreg, two TIF layers were stacked to introduce the two fiber directions. This representation is unable to take into account the direct interaction between the two fiber directions. However, the in-plane shear energy of a dry woven fabric before its locking is very small compared to the energy of the squeeze flow and rotation of viscous prepreg laminate, therefore this assumption is thought to be reasonable.

Due to the use of 3D FEA, the entire stack cannot be computed with a sufficient accuracy on the results due to the computational cost. The simulations were therefore carried out on an area of interest in the middle of the stack, corresponding to points F and G in the first specimen as presented in Figure 2a and to points A, B, C, D and E in the second specimen as presented in Figure 3a. The number of elements in the plane is 24 x 24, and 49 in the thickness to obtain a sufficient accuracy, leading to a total of 28 224 elements and 775 597 degrees of freedom.

5.1. $\{0, 20, 0\}$ stack

The first test specimen was modeled as six layers of TIF grouped two by two, as can be seen in Figure 9. The bottom and top layers consist of a layer oriented at 0° of thickness 0.3mm and a layer oriented at 90° of thickness 1.1mm to represent the volumetric fraction of fiber orientation in the woven fabric. With the same ratio, the middle layers consist of a layer oriented at 20° of thickness 0.3mm and a layer oriented at -70° of thickness 1.1mm. The orientation of -70° was preferred over 110° for numerical considerations, the fiber reorientation being computed based on the velocity gradient which tends to be unstable. A smaller angle value reduces the instability. The length of each side of the cube is 5mm. A pure resin layer is introduced to model the inter-ply resin-rich on either side of a prepreg sheet.

As can be seen in Figure 10 a solid body rotation appears when the stack is subjected to compression, which is consistent with what was observed experimentally. The values were extracted from the interface between the two TIF for each of the three layers, as it contains both fiber direction. The comparison between the numerical and the experimental values is presented in Table 9, where it is seen that the numerical model is in reasonable agreement with the experimental measurements. The difference can be explained by the stacking of two unidirectional plies to model a woven fabric ply. The solid body rotation is predicted correctly, but this model lacks a bit of accuracy when predicting the angle values for an initial orientation of 20°. Considering that the proper woven prepreg model using a fluid approach has not been developed yet, the double TIF layer is found to be a fairly good approach to model the solid body rotation of the woven fabric.

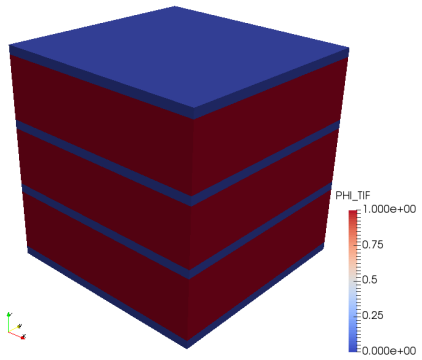

Figure 9. Model of the [0,20,0] specimen. In red (thick layer) are the TIF layers and in blue (thin layer) the resin layers

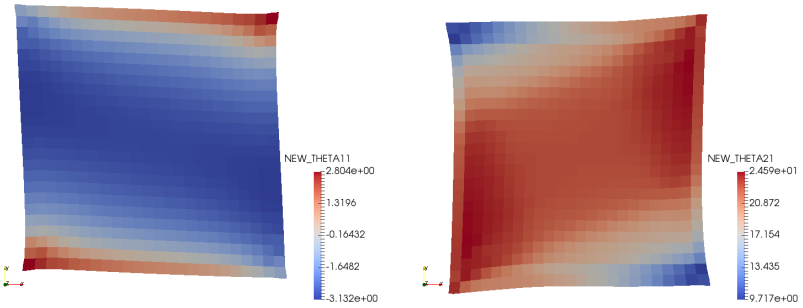

(a) Bottom layer.

(b) Middle layer.

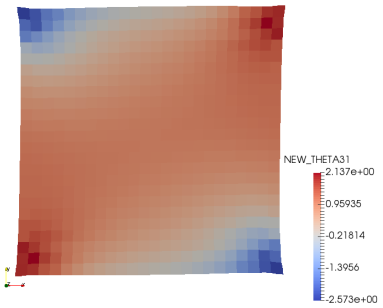

(c) Top layer.

Figure 10. Comparison of the deformed interfaces for the [0,20,0] specimen. Angles are expressed in °

Table 9. Computed angles for a 20 ° intial orientation. Comparison between experimental and numerical values. The total numerical value is the difference of angle between the middle layer and the outer ones

Experimental	5.6
Bottom layer	-3
Middle layer	4.6
Top layer	2
Numerical total	4.1

5.2. $\{0, 80, 0\}$ stack

The second test specimen was modeled as six layers of TIF grouped two by two, as can be seen in Figure 9, just as the first specimen. The bottom and top layers consist of a layer oriented at 0° of thickness 0.3mm and a layer oriented at 90° of thickness 1.1mm to represent the volumetric fraction of fiber orientation in the woven prepreg. With the same ratio, the middle layers consist of a layer oriented at 80° of thickness 0.3mm and a layer oriented at -10° of thickness 1.1mm. The orientation of -10° was preferred over 170° for the numerical reason previously mentioned. The length of each side of the cube is 5mm. As for the previous specimen, a resin layer is introduced between the prepreg layers.

As can be seen in Figure 11 a solid body rotation occurs when the stack is subjected to compression, just as with the previous specimen. The values were extracted from the interface between the two TIF for each of the three layers, as it contains both fiber direction. The comparison between the numerical and the experimental values is presented in Table 10. The numerical predictions match fairly well the experimental observations. Again the difference can be explained by the stacking of two unidirectional plies to model a woven fabric ply. The solid body rotation is predicted correctly, but this model lacks a bit of accuracy when predicting the angle values for an initial orientation of 80°.

Table 10. Computed angles for 80 ° initial orientation. Comparison between experimental and numerical values. The total numerical value is the difference of angle between the middle layer and the outer ones

Experimental	-3.14
Bottom layer	-2.2
Middle layer	-0.2
Top layer	-0.1
Numerical total	-0.95

It is worth to note that the experimental observations showed that the $\{0, 20, 0\}$ stack opens and that the $\{0, 80, 0\}$ stack closes, and that this behavior is predicted correctly by the TIF model.

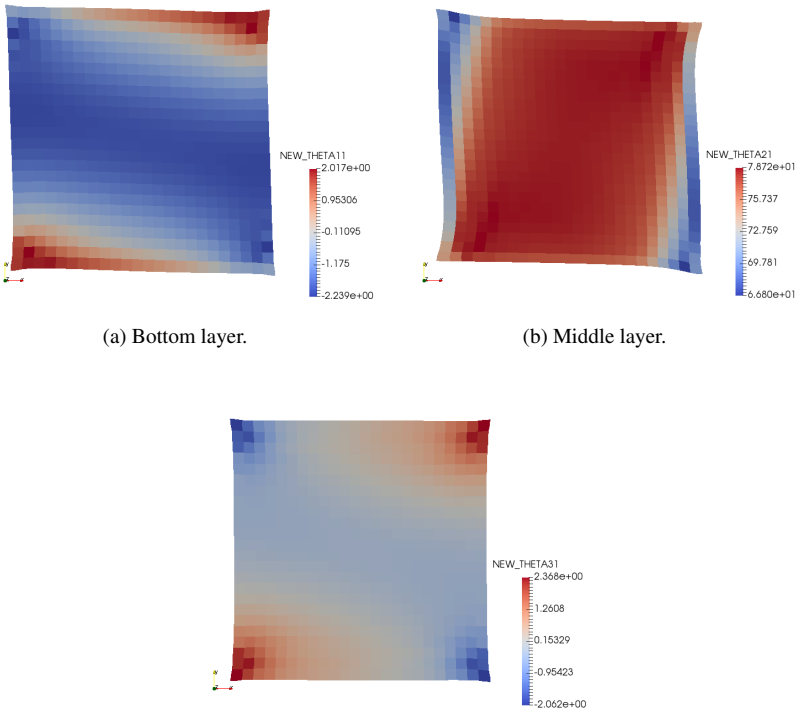

(a) Bottom layer.

(b) Middle layer.

(c) Top layer.

Figure 11. Comparison of the deformed interfaces for the [0,80,0] specimen. Angles are expressed in °

6. Conclusion

It was shown in this paper that a stack of discontinuous viscous unbalanced woven prepregs subjected to through-thickness compression leads to solid body rotation, mainly of the middle layer. Almost no solid body rotation is measured in balanced woven prepreg stacks. A TIF model previously developed to address the squeeze flow in unidirectional viscous prepregs was used here. This choice is first justified by the strong unbalance of the woven structure reinforcing the viscous prepreg. This woven prepreg lies between the unidirectional and balanced woven prepreg. The second reason arises from the use of finite size discontinuous prepregs where no intra-ply shear is observed during transverse squeeze flow.

Numerical simulations showed that although the results are not strictly accurate, the TIF model can be used as a good indicator of the presence of solid body rotation during the through-thickness compression. It can also give a comparative value of the rotation of the plies as it was able to predict correctly the direction of rotation.

Further work in this domain could be the development of a dedicated woven prepreg model based on the anistropic fluid approach as it is very efficient and accurate as discussed in (Sorba *et al*., 2016). Also, the development of a method that would reduce the computational cost would be of great interest.

Acknowledgements

The authors would like to thank the DuPont company for providing the prepreg material.

References

Cogswell F. N. (2013). *Thermoplastic aromatic polymer composites: a study of the structure, processing and properties of carbon fibre reinforced polyetheretherketone and related materials*. Elsevier.

Ghnatios C., Abisset-Chavanne E., Binetruy C., Chinesta F., Advani S. (2016). 3d modeling of squeeze flow of unidirectionally thermoplastic composite inserts. *AIP Conference Proceedings*, Vol. 1769, No. 1, pp. 170002. Retrieved from http://aip.scitation.org/doi/abs/10.1063/1.4963558

Guillon D., CO D., Priem C., Martin A., Rozycki P. (2016, June). A biphasic model to predict the compression strength of misaligned thermoplastic composite. In *17th European Conference on Composite Materials - ECCM17*. Munich, Germany. Retrieved from https://hal.archives-ouvertes.fr/hal-01357301

Hughes T. J. R. (1974). Finite element analysis of incompressible viscous flows by the penalty function formulation. *Journal of Computational Physics*, Vol. 30, pp. 1–60.

McEntee S., Ó Brádaigh C. (1998). Large deformation finite element modelling of single-curvature composite sheet forming with tool contact. *Composites Part A: Applied Science and Manufacturing*, Vol. 29, No. 1, pp. 207–213.

McGuinness G., Ó Brádaigh C. (1997). Development of rheological models for forming flows and picture-frame shear testing of fabric reinforced thermoplastic sheets. *Journal of Non-Newtonian Fluid Mechanics*, Vol. 73, No. 1, pp. 1–28.

Pipkin A. C., Rogers T. G. (1971). Plane deformations of incompressible fiber-reinforced materials. *Journal of Applied Mechanics*, Vol. 38, No. 3, pp. 634. Retrieved from https://doi.org/10.1115%2F1.3408866

Rogers T. (1989). Rheological characterization of anisotropic materials. *Composites*, Vol. 20, No. 1, pp. 21 - 27. Retrieved from http://www.sciencedirect.com/science/article/pii/0010436189906770

Schell J., Amory L., Guillon D., Chinesta F., Cueto E., Abisset-Chavanne E. (2016). Movement of patches during thermoforming: Experiment and simulation. In *Aip conference proceedings*, Vol. 1769, p. 170032.

Sorba G., Binetruy C., Chinesta F. (2016). In-plane shearing of a ud prepreg modeled as transversely isotropic fluid: Comparison between continuous and discontinuous fiber tension approaches. In *Aip conference proceedings*, Vol. 1769, p. 170008.

Spencer A. (1972). *Deformations of fibre-reinforced materials*. Clarendon Press. Retrieved from https://books.google.fr/books?id=uqdRAAAAMAAJ